FISEVIER

Contents lists available at ScienceDirect

# Journal of Hazardous Materials

journal homepage: www.elsevier.com/locate/jhazmat



# Removal of gaseous toluene by the combination of photocatalytic oxidation under complex light irradiation of UV and visible light and biological process

Zaishan Wei\*, Jianliang Sun, Zhirong Xie, Mingyan Liang, Shangzhi Chen

School of Environmental Science and Engineering, Sun Yat-sen University, Guangzhou 510275, China

#### ARTICLE INFO

Article history:
Received 12 June 2009
Received in revised form
30 November 2009
Accepted 26 December 2009
Available online 7 January 2010

Keywords:
Photocatalytic
Biofilter
Toluene
UV and visible light (VL) irradiation
N-TiO<sub>2</sub>/zeolite photocatalyst

#### ABSTRACT

Photocatalysis is a promising technology for treatment of gaseous waste; its disadvantages, however, include causing secondary pollution. Biofiltration has been known as an efficient technology for treatment volatile organic compounds (VOCs) at low cost of maintenance, and produces harmless by-products; its disadvantages, include large volume of bioreactor and slow adaptation to fluctuating concentrations in waste gas. A bench scale system integrated with a photocatalytic oxidation and a biofilter unit for the treatment of gases containing toluene was investigated. The integrated system can effectively oxidize toluene with high removal efficiency. The photocatalytic activity of N-TiO<sub>2</sub>/zeolite was evaluated by the decomposition of toluene in air under UV and visible light (VL) illumination. The N-TiO<sub>2</sub>/zeolite has more photocatalytic activity under complex light irradiation of UV and visible light for toluene removal than that of pure TiO<sub>2</sub>/zeolite under UV or visible light irradiation. N-TiO<sub>2</sub>/zeolite was characterized by scanning electron microscopy (SEM), X-ray photoelectron spectrum analysis (XPS), Fourier transform infrared spectroscopy (FT-IR), and as-obtained products were identified by means of gas chromatography/mass spectrometry (GC/MS). Results revealed that the photocatalyst was porous and was high photoactive for mineralizing toluene. The high activity can be attributed to the results of the synergetic effects of strong UV and visible light absorption, surface hydroxyl groups. The photocatalytic degradation reaction of toluene with the N-TiO<sub>2</sub>/zeolite follows Langmuir-Hinshelwood kinetics. Toluene biodegradation rate matches enzymatic oxidation kinetics model.

© 2010 Elsevier B.V. All rights reserved.

## 1. Introduction

Volatile organic compounds (VOCs) are emitted from a wide range of industries such as chemical, petrochemical, pharmaceutical, food processing, pulp and paper mills, colour printing and painting works [1]. Exposure to VOCs might cause toxic effects to central nervous system and internal organs, and might cause symptoms, such as the sick building syndrome (SBS) including mucous membrane irritation, headache, fatigue, respiratory tract irritation, dizziness and nausea [2–6]. Toluene is a hydrophobic compound and one of the 189 hazardous air pollutants (HAPs) listed in the 1990 Clean Air Act Amendment (CAAA90) proposed by the US Environmental Protection Agency (EPA) [7].

Photochemical oxidation (PCO) is a promising technology which utilizes semiconductors like TiO<sub>2</sub>, ZnO, WO<sub>3</sub>, FeTiO<sub>3</sub>, and SrTiO<sub>3</sub> to carry out a photo-induced redox process that may degrade volatile organic compounds in gaseous phase [8]. The miniaturized photocatalytic air purifier including a continuous adsorption/desorption unit with a zeolite particles-loaded honeycomb rotor can reduce

the toluene concentration in the 1 m<sup>3</sup> room to a value near zero in the first 10-15 min [9]. Photocatalytic oxidation of toluene in the gas-phase was investigated over UV-illuminated thin layer of titanium dioxide [10], spray-hydrolytic synthesis of highly photoactive mesoporous anatase nanospheres [11], TiO2, Pt/TiO2 and Ag/TiO<sub>2</sub> [12]. Photocatalytic activity of both commercial and homemade TiO<sub>2</sub> samples was tested for the degradation of toluene in the gas-phase by using two different irradiation sources, UV and solar [13]. Improving the activities of TiO<sub>2</sub>-based photocatalysts has been attempted by increasing the external surface area, modifying the structural, the morphological or the surface properties, generating defects, modifying the catalyst with metals and coupling semiconductors [14-17]. Recently, C, N, S, F, B anion-doped TiO<sub>2</sub> photocatalysts that show a relatively high level of activity under visible-light irradiation have been reported [18-22]. The feasibility of applying visible light-induced TiO2 doped with N element to cleanse air VOCs at a low ppb concentration commonly associated with IAQ issues [23]. Clay-supported TiO<sub>2</sub> photocatalysts can potentially improve the performance of air treatment technologies via enhanced adsorption and reactivity of target volatile organic compounds [24]. Toluene conversion was up to 90-100% with a slight influence of inlet concentration, whereas flow rate was found to be a prevalent factor [25]. Multi-type N-doped TiO2 was pre-

<sup>\*</sup> Corresponding author. Tel.: +86 20 84037096; fax: +86 20 39332690. E-mail address: weizaishan98@163.com (Z. Wei).

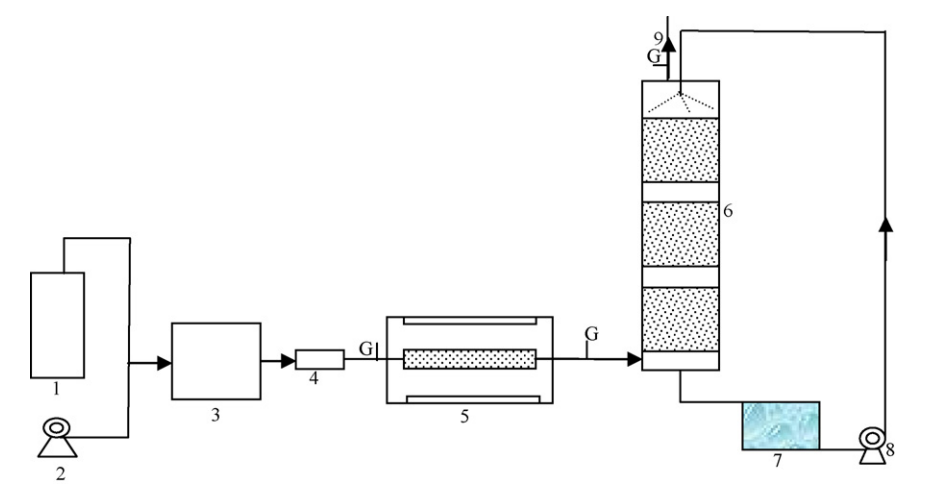


**Fig. 1.** Experimental flow loop of photocatalytic biodegradation of gas-phase toluene. (1) Toluene gas cylinder; (2) air compressor; (3) the bottle of gas mixture; (4) flow mete; (5) photocatalytic reactor; (6) biofilter column; (7) nutrient tank; (8) peristaltic pump; (9) outlet port; (G) sampling port.

pared by thermal decomposition of titanium hydroxide and urea mixtures, the visible light induced toluene photocatalytic activity of TiO<sub>2</sub>–Nw sample was much higher than those of TiO<sub>2</sub>–Nd and TiO<sub>2</sub>–Nh samples and Degussa P25 [26].

Biofiltration has been known as an efficient waste gas control technology for treatment VOCs at low cost of maintenance, and produces harmless by-products. The biofiltration of toluene was studied by some previous researchers [27-30]. Toluene can be effectively treated in a composite membrane bioreactor with a selected aerobic mixed culture [31] or a laboratory-scale biofilm membrane bioreactor inoculated with Burkholderia vietnamiensis G4 [32]. But, photocatalysis may cause secondary pollution during the photocatalysis degradation, various intermediates are formed and some of them can be more toxic and in some cases more persistent than the parent compound [33]; the main by-products in the gas-phase resulting from photocatalytic oxidation of toluene were benzaldehyde, methanol, acetaldehyde, acetone/propionaldehyde, formic acid/ethanol and acetic acid, benzoic acid, hydroguinone, benzylic alcohol, and cresols [34-35]. The biofilter process may run instability and slow adaptation to fluctuating concentrations in waste gas, thus decrease the VOCs removal efficiency due to environmental conditions. This requires combination of photocatalysis and biofiltration technologies to meet the strict standards.

In this study, an integrated reactor, consisting of a photocatalytic oxidation unit and a biofiltration unit, was used to treat waste gaseous containing toluene. The objectives were to further improve the efficiency of toluene removal by integrating photocatalytic oxidation and biological processes, to eliminate secondary pollution and to run stability. The study analysis characterize of N-TiO<sub>2</sub>/zeolite, and evaluates the factors such as photocatalytic activity, empty bed residence time (EBRT), inlet concentration, catalyst and biological oxidation on the performance of the photocatalytic-biological system, the mechanistic and the kinetics for photocatalytic-biological oxidation of toluene were elicited.

#### 2. Materials and methods

### 2.1. Preparation of N-TiO<sub>2</sub>/zeolite

The N-doped titanium dioxide ( $TiO_2$ ) was prepared by the sol-gel method. 50 mL  $Ti(OC_4H_9)_4$  was dissolved in 350 mL absolute ethyl alcohol, using 20 mL acetic acid as gel depressant under magnetic stirring for 45 min to obtain a transparent gel colloid. 3 g urea was dissolved in 30 mL deionized water, adding into 150 mL absolute ethyl alcohol and 20 mL acetic acid to get a solution. Then

the solution was dropped into the gel colloid under magnetic stirring for 2 h, the mixture was agitated for 24 h in room temperature. Undoped TiO<sub>2</sub> was prepared by the same method and materials, without using urea as starting materials. This TiO<sub>2</sub> photocatalysts were loaded in Ca-5A zeolite (external diameter of 3–4.6 mm) by impregnation method. The N-TiO<sub>2</sub>/zeolite photocatalyst was dried in the drying oven at 85 °C for 60 min, and placed in the middle of muffle furnace, calcined at 400 °C for 60 min. After cooling to room temperature, the samples were taken out for further investigations.

## 2.2. Physico-chemical characterization of N-TiO<sub>2</sub>/zeolite

The N-TiO<sub>2</sub>/zeolite was then examined by scanning electron microscopy (SEM) with a electron detector (Japan, JSM-6330F). Surface element analysis was carried out by X-ray photoelectron spectrum analysis (XPS) using a Thermo ESCALAB 250 instrument with Al K $\alpha$  radiation ( $h\nu$  = 1486.6 eV) at 150 W. The signal of adventitious carbon (a binding energy of 284.8 eV) has been used to calibrate the binding energy scale for X-ray photoelectron spectrum analysis (XPS) measurements. The UV-vis absorbance spectra were obtained for the dry-pressed disk samples using a Scan UV-vis spectrophotometer (UV-2501PC, Japan) equipped with an integrating sphere assembly, using BaSO<sub>4</sub> as reflectance sample. Fourier transform infrared spectroscopy (FT-IR) (EQUINOX 55, Bruker Co.) analyses were used to identify the intermediate products at room temperature.

## 2.3. Experimental procedure

The flow loop used in the study is shown schematically in Fig. 1. The bench-scale integrated reactor system includes a photocatalytic reactor and a biofilter. The toluene supplied from the gas cylinders, was first diluted with the compressed air, passed through an air mixture bottle, then flowed through the photocatalytic reactor and flowed upwards the bottom of the biofilter. Photocatalytic experiments were carried out using the photocatalytic reactor packed with N-TiO<sub>2</sub>/zeolite (external diameter of 3-4.6 mm) 40 mm in diameter and 100 mm in working height. The N-TiO<sub>2</sub>/zeolite was exposed to a luminous source composed of a 4W UV-lamp (the wavelength maximum of the light source was 253.7 nm), 4W visible light-lamp, placed in axial position. The biofilter column (internal diameter of 90 mm and 1200 mm long) was packed with ceramsite (external diameter of 8-15 mm) to a height of 510 mm, which was set up to study removal of toluene from stimulated waste gas. It was divided into three sections with

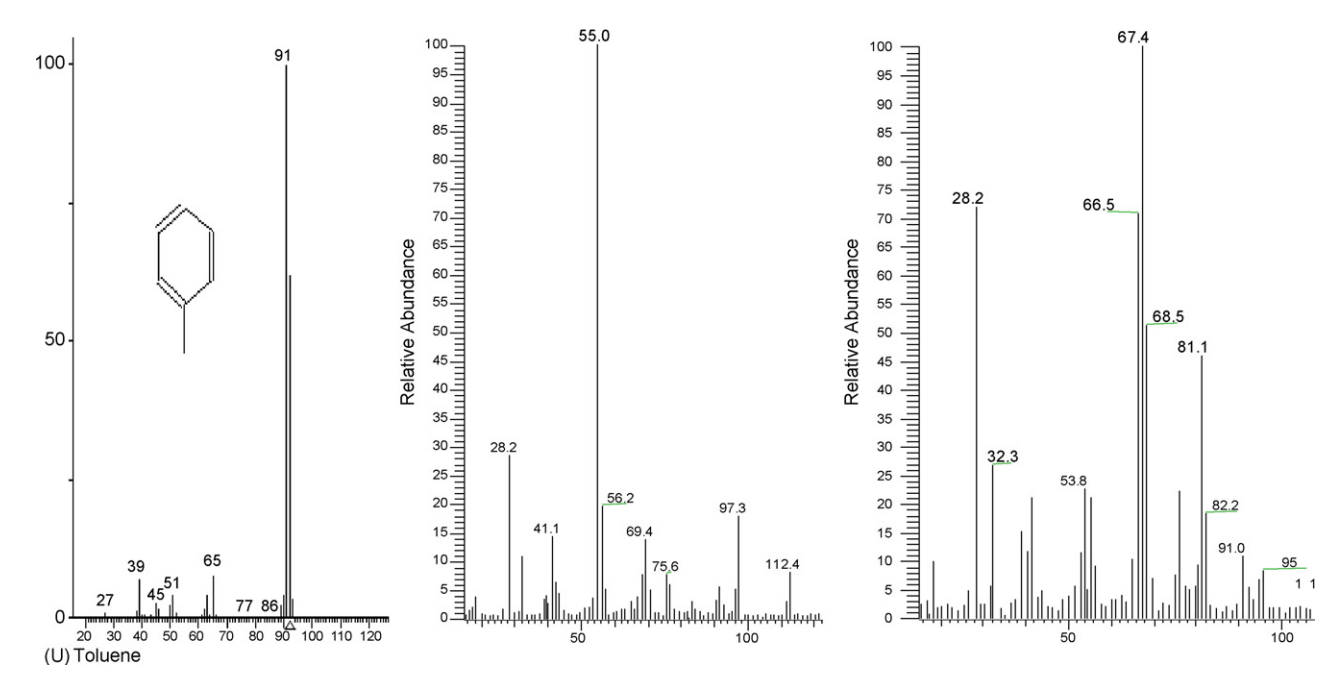


Fig. 2. Gas chromatographic-mass spectra of analysis of outlet stream samples from toluene photooxidation over N-TiO<sub>2</sub>/zeolite catalyst.

the filter medium at each section was supported on a stainless steel sieve plate that ensured homogeneous distribution of gas flow over the entire cross section of the filter bed; biodegrading bacterials adhere to the surface of ceramsite to form the biofilm, the microbial inoculum culture was obtained by acclimating the activated sludge taken from the local wastewater treatment plant. Toluene concentrations were monitored by the analysis device of Photo-Ionization Detector, and gas flow rate was monitored by the rotameter and the mass flow controllers. In the process of the biodegradation of toluene experiments, nutrient-containing aqueous solutions was sprayed downward at a rate of 2.81-45 Lh<sup>-1</sup> with a peristaltic pump from the top of column to maintain the moisture of the biofilter and supply nutrients to the microbial population. The simulated toluene-containing waste gas was supplied to the photocatalytic reactor and the biofilter, at a flow rate of 100-300 Lh<sup>-1</sup> (EBRT, 40.4-121.3 s).

#### 2.4. Analytical methods

Periodic measurements of toluene concentration from sampling ports and gas flow rate in the photocatalytic-biological integrated reactor system were carried out using the following devices. Mini-RAE PLUS PGM-76 Photo-Ionization Detector analysis device was used for analysis of toluene concentration, which was made in USA. Gas flow rates were measured using Model LZB-1 flow meters with units of 1 L h<sup>-1</sup>. The pH values were measured by a Model pHB-3 pH Tester (Sanxin Instrument Company, Shanghai, China).

#### 2.5. Confirmation of the reaction products by GC-MS

The photooxidation intermediate products were identified by analysing them with a GC-MS (Thermo-Finnegan). The GC-MS chromatogram and mass patterns for each compound are depicted in Fig. 2. The gas-phase intermediate organic products were detected in the sample after the photoreaction. While toluene (PhCH<sub>3</sub>, m/z=91) was identified in the sample collected before photoreaction, the gas-phase intermediate organic products such as methyl glyoxal (CH<sub>3</sub>COCHO, m/z=55) and vinyl methyl ketone

 $(CH_2=CH-COCH_3, m/z=68)$  were detected in the sample after photographics.

#### 3. Results and discussion

### 3.1. Catalyst characterization

## 3.1.1. XPS analysis

The fine crystal of nanoscale N-TiO $_2$ /zeolite is conglomerated and the surface of the N-TiO $_2$ /zeolite sample is found to be porous (Fig. 3). N-TiO $_2$ /zeolite has optimal pore distribution for adsorption toluene.

Photoelectron spectra of Ti2p, N1s, O1s levels for N-TiO<sub>2</sub>/zeolite after the reaction are displayed in Fig. 4. High-resolution scan over Ti2p peaks showed that the binding energy of Ti2p was 458.7 eV, which indicated that Ti loaded on the catalyst existed as TiO<sub>2</sub>. According to the N1s peaks, the observed peak at 400.3 eV is due to the presence of substitutional N in oxidized nitrogen state such as Ti–N–O linkages. Theoretical studies about N-doped TiO<sub>2</sub> have been performed by Di Valentin et al. [36] to clarify the origin of visible light activity. The peak of O1s could be well fitted as a combination of N–O (peak at 530.3) and the OH– groups (peak at 531.8) [37]. Hydroxyl groups (–OH) results mainly from the chemisorbed water [38].

## 3.1.2. Optical characteristics

The UV–vis diffuse reflectance spectra of N–TiO<sub>2</sub>/zeolite after the reaction are shown in Fig. 5. The spectra of N–TiO<sub>2</sub>/zeolite consisted of a single and broad intense absorption around 400 nm due to a charge-transfer transition between the lattice oxygen ligands ( $\rm O^{2-}$ ) and a central titanium ion ( $\rm Ti^{4+}$ ) with octahedral coordination. A broad band between 450 and 650 nm centered at 535 nm could be observed in the absorption spectra of N–TiO<sub>2</sub>/zeolite owing to a transition of N–O particles. The N–TiO<sub>2</sub>/zeolite shows an onset of absorption at 400 nm as commonly observed, while doping of N effectively extends the absorption edge into the visible light region. N doping contributed to the localized N1s states, which are responsible for visible light absorption [39].

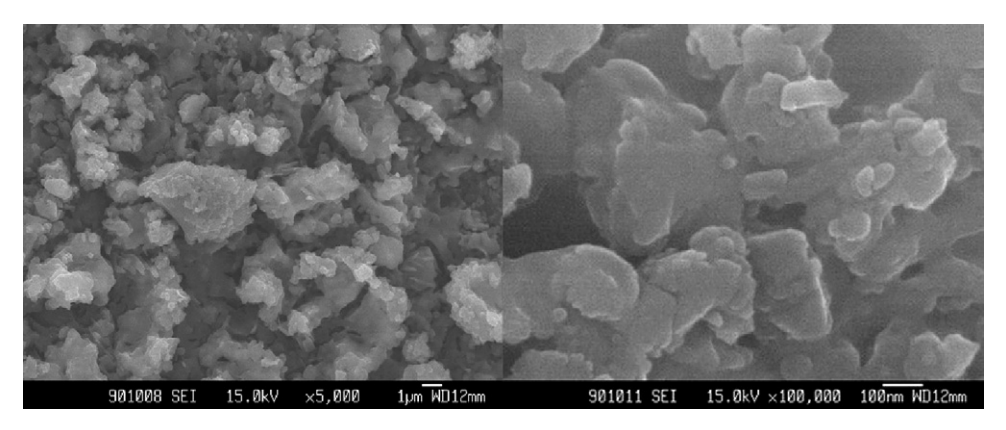


Fig. 3. SEM images of N-TiO<sub>2</sub>/zeolite.

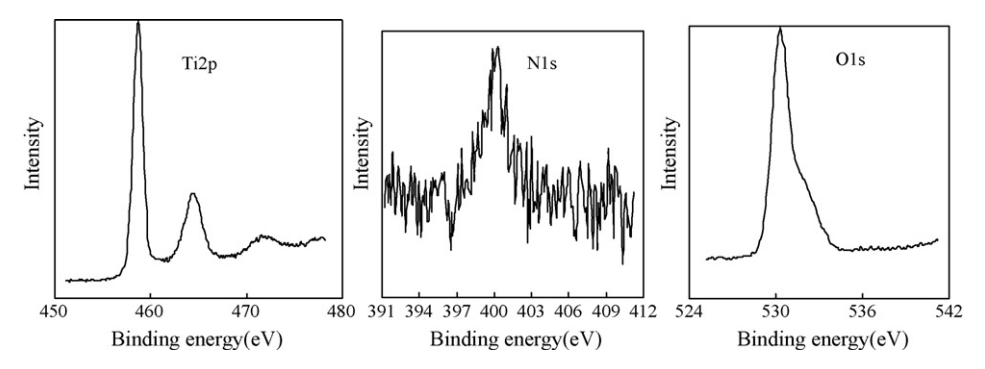


Fig. 4. XPS spectra of the core levels for N-TiO<sub>2</sub>/zeolite after the reaction.

## 3.1.3. FT-IR analysis

In Fig. 6, we show the FT-IR spectra of N-TiO $_2$ /zeolite samples in the range  $4000-500\,\mathrm{cm}^{-1}$ . Within the range  $3500-2800\,\mathrm{cm}^{-1}$  it shows up the bands corresponding to surface hydroxyl groups. Two clear bands can be observed in both series, one located at  $3392\,\mathrm{cm}^{-1}$  and a second one located around  $3101\,\mathrm{cm}^{-1}$ . These bands can be attributed to the different OH groups at the surface.

FT-IR spectra of N-TiO $_2$ /zeolite are shown in Fig. 4. The band at 3430–3410 cm $^{-1}$  corresponds to the O–H stretching vibration, while the band at 1640–1631 cm $^{-1}$  results from O–H bending of adsorbed (toluene) water molecules. The band below 1000 cm $^{-1}$  corresponds to the titania crystal lattice vibration [40–41]. The new weak components appear at 1667, 1480, and 1449 cm $^{-1}$ , and a slight increase in intensity of the 1600 cm $^{-1}$  band occurs. This suggests that a fraction of toluene molecules are transformed into new species under complex light of UV and VL irradiation.

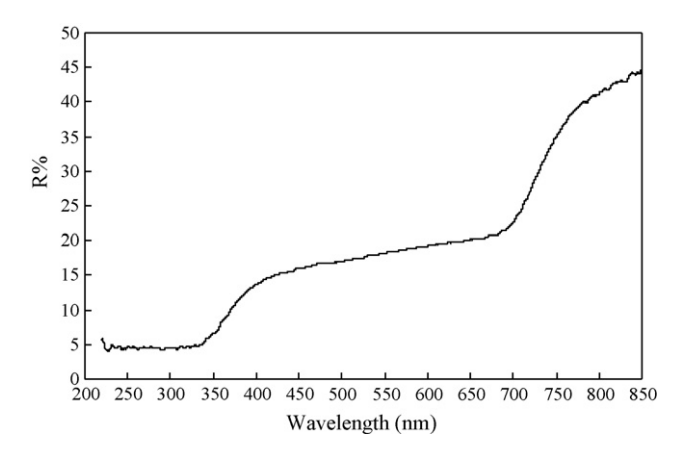
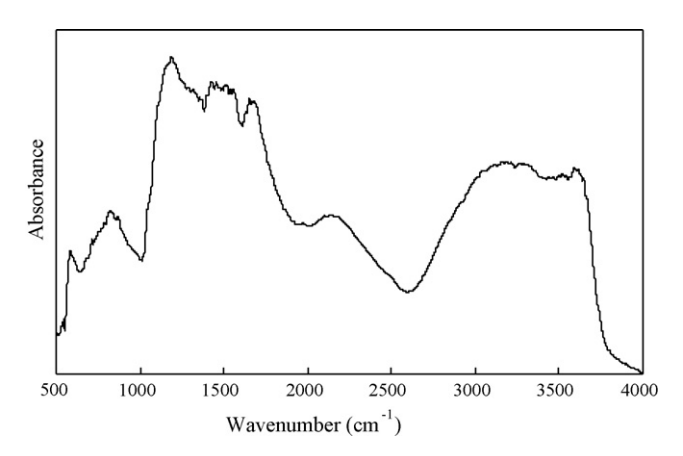


Fig. 5. UV-vis diffuse reflectance spectra of the N-TiO<sub>2</sub>/zeolite catalyst.

## 3.2. Photocatalytic activity of N-TiO<sub>2</sub> /zeolite

The photocatalytic oxidation of toluene was performed in order to investigate the photocatalytic activity of N-TiO<sub>2</sub>/zeolite and TiO<sub>2</sub>/zeolite under UV, visible light (VL) or complex light of UV and VL. There is obvious significant raise in photocatalytic activity between N-TiO<sub>2</sub>/zeolite and TiO<sub>2</sub>/zeolite under UV-light irradiation, and toluene removal efficiency increases from 14.6 to 26.6% (Fig. 7). In the visible light irradiation experiment, it has no effect of the degradation effect with TiO<sub>2</sub>/zeolite, while toluene photocatalytic efficiency could be attained 26.6% with N-TiO<sub>2</sub>/zeolite from 90 min to 120 min. Toluene photocatalytic efficiency increases from 14.3 to 62.5% when increasing the illumination time from 15 min to 120 min using N-TiO<sub>2</sub>/zeolite under complex light irradiation of UV and visible light (Fig. 2), the equilibrium efficiency attained 58.9% after from 5 d to 6 d longer irradiation time (Fig. 8). The



**Fig. 6.** FT-IR spectrum of N-TiO<sub>2</sub>/zeolite after photocatalytic reaction.

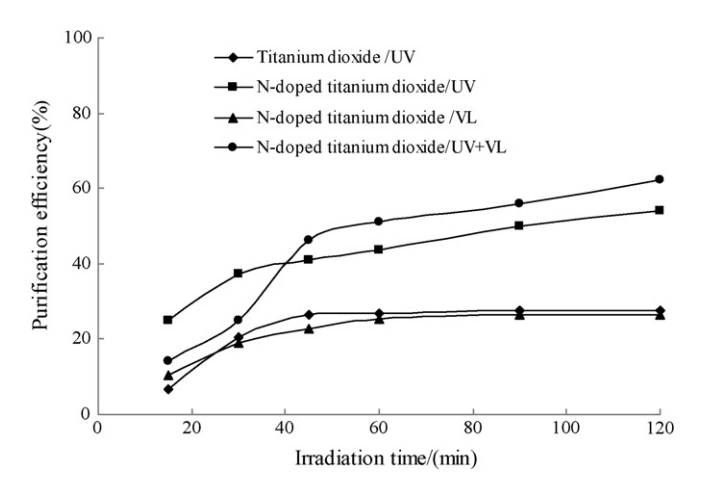


**Fig. 7.** Photocatalytic activity of N-TiO<sub>2</sub>/zeolite under complex light of UV and VL irradiation (experimental conditions: EBRT =  $4.5 \, \text{s}$ , inlet concentration of  $290 \, \text{mg m}^{-3}$ ).

best toluene removal efficiency could be achieved 62.5% at 120 min under EBRT of 4.5 s, inlet concentration of 290 mg m $^{-3}$ . For comparison, toluene photocatalytic degradation effect of the experiment using N-TiO<sub>2</sub>/zeolite under complex light irradiation of UV and VL is much higher than that using N-TiO<sub>2</sub>/zeolite under UV irradiation. The performance of N-TiO<sub>2</sub>/zeolite is better under combination of UV and VL than that under UV alone, N-TiO<sub>2</sub>/UV has the same performance as TiO<sub>2</sub>-UV, the possible reason for this could be that the feasibility of applying visible light-induced TiO<sub>2</sub> doped with N element to cleanse air toluene. The zeolite support adsorption toluene to photocatalytic oxidation toluene. TiO<sub>2</sub> may carry out a photo-induced redox process that may degrade toluene in gaseous phase.

### 3.3. Performance of the integrated system

Toluene photocatalytic efficiency of changes slight from 53 to 58.2% before 14 d, then decreases from 56.3% at 14th d to 34.1% at 17th d, this illustrated that N-TiO $_2$ /zeolite has good photocatalytic activity under complex light of UV and visible light irradiation for 13 d (Fig. 8). The possible reason for the fall in photocatalytic efficiency beyond 13 d could be that photocatalytic activity of N-TiO $_2$ /zeolite is losing. Therefore, the N-TiO $_2$ /zeolite must be regenerated for reuse. The conversion of toluene biodegradation

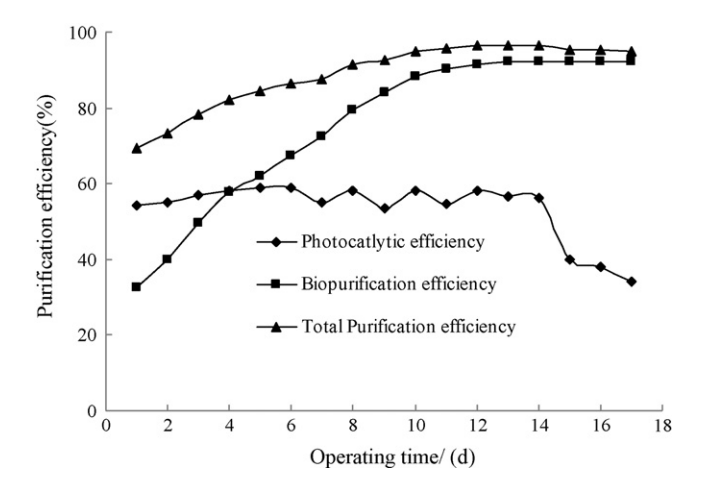


**Fig. 8.** performance of the integrated reactor during the 17-d continuous running test (experimental conditions: sprinkling amount from 1.7 to  $45 \, \text{Lh}^{-1}$ ; pH 7.1–7.4; environmental temperature =  $21 \, ^{\circ}\text{C}$ ; EBRT =  $121.3 \, \text{s}$ , inlet concentration from 210 to  $500 \, \text{mg m}^{-3}$ ).

efficiency increases from 32.7% with 1 d to 92.3% at 17th d, whereas the conversion of total toluene removal efficiency increases from 69.3 to 96.7%, then decreases to 94.9%, showing good toluene degradation effect. The N-TiO<sub>2</sub>/zeolite should be replaced to improve the general process beyond the ripening period of the biological process (>12 d). Obviously, the photocatalytic process yield to bifiltration after the 4th d. Furthermore, the photocatalytic process reached the steady-state condition faster than the biofilter by 2.5 times. This indicates that the design of the biofilter is also essential to the overall performance of the integrate treatment system. Because toluene solubility is small in water, the scrubbing effect of water could hardly play a role in toluene removal, toluene is oxidized to carbon dioxide, water vapors by biological oxidation at the steady-state in biofiltration process, toluene biodegradation efficiency remain attained 92% maintaining adequate moisture in the filter bed without supply of water from the top of bioreactor. Toluene biodegradation efficiencies were 90-98% with inlet concentrations of 60–500 mg m<sup>-3</sup> for 300-d long-term operating

The photocatalytic degradation of toluene on the N-TiO<sub>2</sub>/zeolite follows three steps: (1) the adsorption of toluene molecules onto the surface of N-TiO<sub>2</sub>/zeolite; (2) a fast inducement by the complex light irradiation of UV and visible light, which includes the produce of electron-hole pairs, hydroxyl radicals and likely oxidation; the photogenerated conduction band electrons were trapped by oxygen molecules, leading to the formation of radicals such as O<sub>2</sub>•, HOO• and •OH to produce active oxidizing species, usually hydroxyl radicals (\*OH) in presence of air, but also dissociated neutral oxygen species  $(0^{\bullet})[2]$ . These free radicals with a high oxidation potential were the predominant species contributing to the degradation of the toluene; (3) the N-TiO<sub>2</sub>/zeolite photocatalytic free radical oxidation of toluene can also proceed in a different way, giving rise to the gas-phase intermediate organic products with N-TiO<sub>2</sub>/zeolite under complex light irradiation of UV and visible light. This gas-phase intermediate organic products such as benzaldehyde ( $C_6H_5CHO$ ), benzene ( $C_6H_6$ ), benzal methanol ( $C_6H_5CH_2OH$ ), formaldehyde (HCHO), methyl vinyl ketone and methyl glyoxal were detected during the photocatalytic-degradation of toluene

Toluene (PhCH<sub>3</sub>), the intermediate organic products such as benzaldehyde (C<sub>6</sub>H<sub>5</sub>CHO), benzene (C<sub>6</sub>H<sub>6</sub>), benzal methanol (C<sub>6</sub>H<sub>5</sub>CH<sub>2</sub>OH), formaldehyde (HCHO), vinyl methyl ketone (CH<sub>2</sub>=CH-COCH<sub>3</sub>) and methyl glyoxal (CH<sub>3</sub>COCHO) are converted to CO<sub>2</sub> and H<sub>2</sub>O through biological oxidation reaction. In the biofilter, toluene air stream is forced to pass through a ceramsite support material on which pollutant-degrading cultures are immobilized. Toluene and oxygen diffuse from the gas-phase to the wet layer of the biofilm and then are consumed by the microorganism communities. Under aerobic conditions in a biofilter, toluene and these compounds are oxidized to carbon dioxide, water vapors by biological oxidation; toluene solubility is small in water due to its low Henry's constants, mass transfer limitation may play an important role during biological treatment; gas-phase toluene should first diffuse through a thin aqueous layer surrounding the filter medium, and then toluene is directly adsorption to the surfaced of biofilm, biological oxidation is the process in which toluene is oxidized to  $CO_2$  and  $H_2O$ .

Thus, a bench scale system integrated with a photocatalytic oxidation and a biofilter unit should eliminate secondary pollution from toluene photocatalytic degradation process and run stability.

## 3.4. The influence of empty bed residence time (EBRT)

The effect of EBRT on removal of toluene is presented in Fig. 9, under the conditions of pH of 7.2, inlet concentration of 300 mg m $^{-3}$  toluene and sprinkling amount at 9.5 L h $^{-1}$  in the integrated sys-

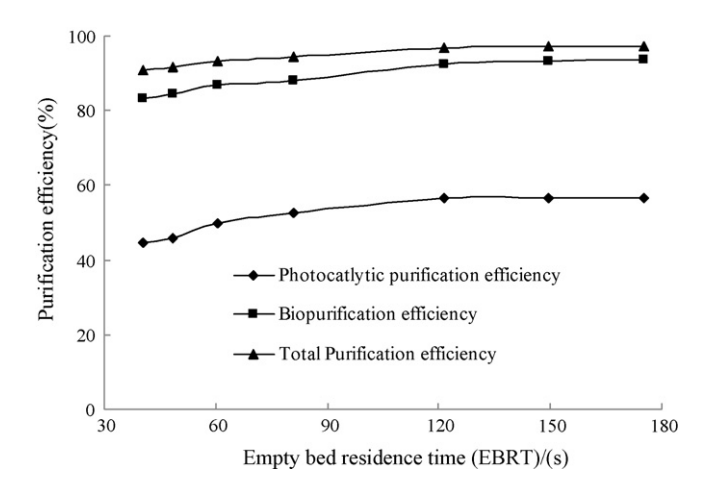


**Fig. 9.** Influence of EBRT on toluene removal (experimental conditions: inlet concentration of  $300\,\mathrm{mg\,m^{-3}}$ , sprinkling amount=9.5 Lh<sup>-1</sup>; pH 7.2; environmental temperature of  $25\,^{\circ}$ C).

tem. Toluene photocatalytic efficiency increases from 44.7 to 56.7%, whereas toluene biodegradation efficiency increases from 83.1 to 93.8%, total toluene removal efficiency increases by 6.6% with EBRT increasing (Fig. 9). This indicates the longer residence time is a benefit on the removal of toluene, in the case where the EBRT is too short to photocatalytic-biological oxidized toluene to  $\rm CO_2$ ,  $\rm H_2O$  before release. The type of photocatalyst, the length of the quartz tube with photocatalyst and UV or visible light, and the volume of biofilter with degradation toluene microorganisms are the key elements. From Fig. 9, in our experimental conditions, we can assume the optimum EBRT is 60.6 s in the integrated system, and about 93% toluene in the gas stream is converted.

# 3.5. The influence of toluene concentration

Keeping EBRT of  $60.6\,\mathrm{s}$ , and sprinkling amount  $(9.5\,\mathrm{L\,h^{-1}})$ , pH of  $7.4\,\mathrm{fixed}$ , the influence of toluene concentration in inlet on removal of toluene with the photocatalytic reactor and biofilter are presented in Fig. 10. The conversion of total toluene removal efficiency reduces from 96.1% with  $210\,\mathrm{mg\,m^{-3}}$  to 92.7% with  $800\,\mathrm{mg\,m^{-3}}$  toluene, the toluene biodegradation efficiency also reduces from 90.8 to 82.9%, whereas toluene photocatalytic efficiency changes slightly within the increasing inlet concentration of toluene from  $210\,\mathrm{to}\,800\,\mathrm{mg\,m^{-3}}$ . More than 96% toluene is

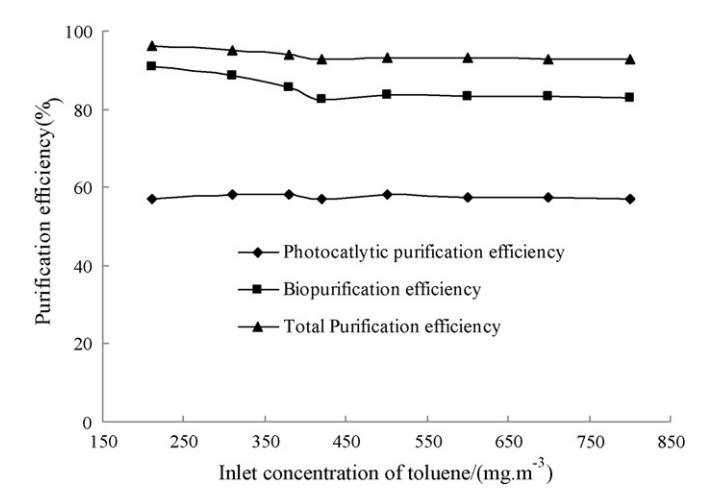


**Fig. 10.** Influence of concentration of toluene in inlet on toluene removal (experimental conditions: sprinkling amount= $9.5 \, \text{Lh}^{-1}$ ; pH 7.4; environmental temperature= $25\,^{\circ}\text{C}$ ; EBRT= $60.6\,\text{s}$ ).

photocatalytic-biological oxidized for less than the initial concentration of  $210 \, \text{mg m}^{-3}$  toluene. Under the conditions of sprinkling amount of  $9.5 \, \text{L} \, \text{h}^{-1}$ , initial toluene concentration of  $120 \, \text{mg m}^{-3}$  and EBRT of  $121.3 \, \text{s}$ , the total toluene removal efficiency could reach 96.7%. This illustrates that the photocatalytic-biological reactor is efficient in purifying the waste gas whose toluene concentration is between  $210 \, \text{and} \, 800 \, \text{mg m}^{-3}$ .

As are shown in Fig. 10, the simultaneous presence of photocatalytic reactor and biofilter increases from 5.2 to 9.4% with increasing toluene concentration in inlet than the biofilter only. The additional use of the biofilter to photocatalytic reactor not only leads to the enhancement of toluene removal efficiency up from 35.2 to 39%, but also eliminates gas-phase intermediate organic products from photocatalytic degradation of toluene to produce CO<sub>2</sub>, H<sub>2</sub>O.

#### 3.6. Kinetic analysis

In the integrated treatment system, part of toluene is photocatalytic oxidized to gas-phase intermediate organic products,  $CO_2$ ,  $H_2O$  using N-TiO $_2$ /zeolite under complex light irradiation of UV and visible light. Langmuir–Hinshelwood (L–H) rate expression is used to describe the gas–solid-phase reaction of photocatalytic degradation of toluene for heterogeneous photocatalysis [6,46]. Toluene and the intermediate organic products are biological oxidized into harmless byproducts such as  $CO_2$ ,  $H_2O$  in the biofilter. Enzymatic oxidation kinetics model is used to describe the toluene biodegradation reaction.

Assuming that the toluene mass transfer is not the limiting step and that the effect of intermediate product is negligible, substrate toluene is adsorption onto the surface of the N-TiO<sub>2</sub>/zeolite photocatalyst. The reaction rate in a photocatalytic reactor can be expressed linearly as:

$$\frac{\ln\left(C_{\rm in}/C_{\rm out}\right)}{C_{\rm in}-C_{\rm out}} = \frac{kK\left(V/Q\right)}{C_{\rm in}-C_{\rm out}} - K \tag{1}$$

where k and K are the L–H reaction rate constant and the L–H adsorption equilibrium constant,  $C_{\rm in}$  and  $C_{\rm out}$  are the inlet and outlet concentrations of toluene, respectively, V is the gas volume of the photocatalytic reactor (49.2 mL); and Q is the flow rate through the reactor (200 L h<sup>-1</sup>).

If L–H model is valid, a plot of  $\ln(C_{\rm in}/C_{\rm out})/(C_{\rm in}-C_{\rm out})$  versus  $1/(C_{\rm in}-C_{\rm out})$  should be linear. The experimental data are in good agreement with the integral rate law analysis and a linear relationship is observed ( $R^2$  = 0.99896). As shown in Fig. 11, the obtained values of k and K are 1476.8 mg m<sup>-3</sup> min<sup>-1</sup> and 0.000106745 (mg m<sup>-3</sup>)<sup>-1</sup>, respectively. This finding suggests that photocatalytic reaction occurs on the photocatalyst surface through L–H mechanism and not in the gas-phase. The photocatalytic toluene rate matches Langmuir–Hinshelwood model in the photocatalytic reactor with N-TiO<sub>2</sub>/zeolite under complex light irradiation of UV and visible light.

The toluene biodegradation rates in the biofilter were calculated using the following equation derived from the Michaelis-Menten equation

$$\frac{1}{R} = \frac{K_s}{V_m} \cdot \frac{1}{C_{ln}} + \frac{1}{V_m} \tag{2}$$

where R (g-toluene m<sup>-3</sup> h): apparent removal rate;  $C_{\rm ln}({\rm g\,m^{-3}}) = (C_{\rm in}-C_{\rm out})/{\rm ln}(C_{\rm in}/C_{\rm out})$ , logarithmic mean concentration of toluene at the inlet and outlet of the biofilter;  $V_{\rm m}$  (g-toluene m<sup>-3</sup> h<sup>-1</sup>): maximum apparent removal rate and  $K_{\rm s}$  (g m<sup>-3</sup>): apparent half-saturation constant. From the linear relationship between  $1/C_{\rm ln}$  and 1/R,  $V_{\rm m}$  and  $K_{\rm s}$  were calculated from the slope and intercept. In this experiment, the flow rates were controlled in the range of  $200\,{\rm L\,h^{-1}}$ .

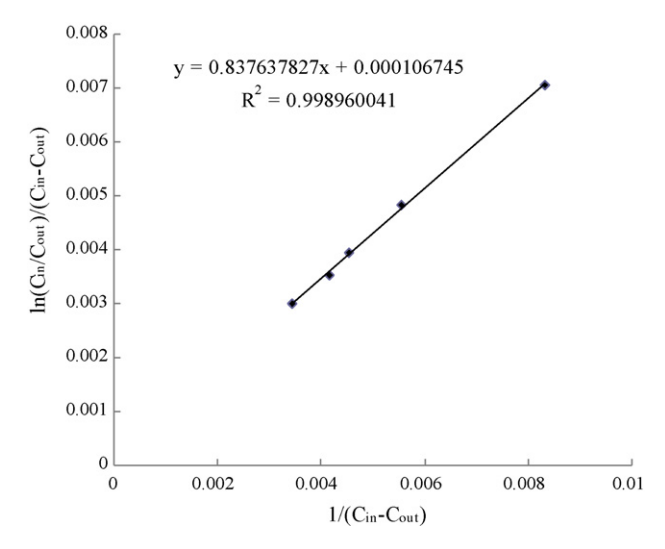


**Fig. 11.** Plot of  $\ln(C_{\rm in}/C_{\rm out})/(C_{\rm in}-C_{\rm out})$  versus  $1/(C_{\rm in}-C_{\rm out})$  according to the L–H photocatalytic gradation toluene rate expression (experimental conditions: inlet concentration of 210–500 mg m<sup>-3</sup>; EBRT = 2.3 s, gas flow rate of 200 L h<sup>-1</sup>).

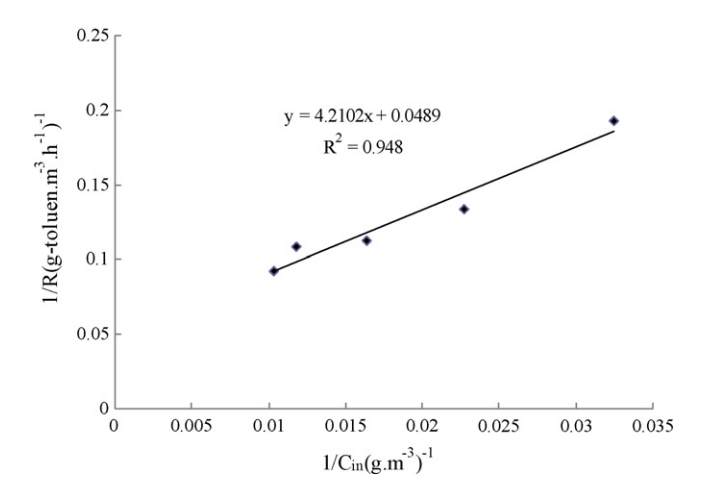


**Fig. 12.** Relationship between 1/R and  $1/C_{\rm in}$ ; toluene degradation in the tricking biofilter (experimental conditions: sprinkling amount = 9.5 Lh<sup>-1</sup>; pH 7.4; environmental temperature = 25 °C; EBRT = 58.4 s).

The kinetic of toluene biodegradation in the range of  $90-210 \,\mathrm{mg}\,\mathrm{m}^{-3}$  toluene concentrations is analysed. As shown in Fig. 12, the experimental data are in good agreement with the integral rate law analysis and a linear relationship is observed ( $R^2=0.948$ ).  $V_{\mathrm{m}}$  and  $K_{\mathrm{s}}$  of toluene were calculated by the Lineweaver–Burk method from the regression equation to be  $20.83 \,\mathrm{g}$ -toluene m<sup>-3</sup> h<sup>-1</sup> and  $87.71 \,\mathrm{g}\,\mathrm{m}^{-3}$ . This indicates that the biofilter has good toluene removal effect. Because toluene solubility is small in water, toluene may be adsorbed to the surface of biomass indirectly, which is biological-degradation to  $CO_2$  and  $H_2O$ .

# 4. Conclusions

The paper revealed that the photocatalytic-biological process can be used for removal of toluene from waste gas, and Langmuir–Hinshewood kinetic model was successfully applied to describe this process on photocatalytic degradation of toluene, toluene biodegradation rate matches enzymatic oxidation kinetics model. The experimental results showed that the toluene removal efficiency could be achieved 96.7% under the feasible conditions. The optimal empty bed residence time (EBRT) is 60.6 s. The N-TiO<sub>2</sub>/zeolite had more photocatalytic activity for removal

of toluene than that of pure  $TiO_2$ /zeolite. The characterizations of  $N-TiO_2$ /zeolite were also conducted to investigate. The photocatalytic biological degradation of technology is a viable and promising method for VOCs control.

#### Acknowledgement

The authors gratefully acknowledge the financial support from the Project Foundation of Guangdong Zhuhai Science & Technology (PC20082029).

#### References

- [1] R.R. Eldon, D.V.S. Murthy, T. Swaminathan, Performance evaluation of a compost biofilter treating toluene vapours, Process Biochem. 40 (2005) 2771–2779.
- [2] K.P. Yu, G.W.M. Lee, Decomposition of gas-phase toluene by the combination of ozone and photocatalytic oxidation process (TiO<sub>2</sub>/UV, TiO<sub>2</sub>/UV/O<sub>3</sub>, and UV/O<sub>3</sub>), Appl. Catal. B Environ. 75 (2007) 29–38.
- [3] J.H. Mo, Y.P. Zhang, Q.J. Xu, J.J. Lamson, R.Y. Zhao, Photocatalytic purification of volatile organic compounds in indoor air: a literature review, Atmos. Environ. 43 (2009) 2229–2246.
- [4] WHO, Indoor air quality: organic pollutants, Report on a WHO meeting, EURO Report and Studies, 1989, 1–70.
- [5] USEPA, Reducing Risk: Setting Priorities and Strategies for Environmental Protection, U.S. Environmental Protection Agency, 1990.
- [6] J. Auvinen, L. Wirtanen, The influence of photocatalytic interior paints on indoor air quality, Atmos. Environ. 37 (2008) 4101–4112.
- [7] Y.H. Liu, X. Quan, Y.Z. Zhao, S. Chen, H.M. Zhao, Removal of ternary VOCs in air streams at high loads using a compost-based biofilter, Biochem. Eng. J. 23 (2005) 85–95.
- [8] K. Demeestere, A. De Visscher, J. Dewulf, M. Van Leeuwen, H. Van Langenhove, A new kinetic model for titanium dioxide mediated heterogeneous photocatalytic degradation of trichloroethylene in gas-phase, Appl. Catal. B Environ. 54 (2004) 261–274.
- [9] F. Shiraishi, T. Ishimatsu, Toluene removal from indoor air using a miniaturized photocatalytic air purifier including a preceding adsorption/desorption unit, Chem. Eng. Sci. 64 (2009) 2466–2472.
- [10] V. Tomašić, F. Jović, Z. Gomzi, Photocatalytic oxidation of toluene in the gas phase: modelling an annular photocatalytic reactor, Catal. Today 137 (2008) 350–356.
- [11] M.H. Zhou, J.G. Yu, S.W. Liu, P.C. Zhai, B.B. Huang, Spray-hydrolytic synthesis of highly photoactive mesoporous anatase nanospheres for the photocatalytic degradation of toluene in air, Appl. Catal. B Environ. 89 (2009) 160–166.
- [12] C. Young, T.M. Lim, K. Chiang, J. Scott, R. Amal, Photocatalytic oxidation of toluene and trichloroethylene in the gas-phase by metallised (Pt, Ag) titanium dioxide, Appl. Catal. B Environ. 78 (2009) 1–10.
- [13] F. Chen, W.W. Zou, W.W. Qu, J.L. Zhang, Photocatalytic performance of a visible light N-TiO<sub>2</sub> prepared by a surface chemical modification process, Catal. Commun. 10 (2009) 1510–1513.
- [14] C. Martín, G. Solana, V. Rives, G. Marcì, L. Palmisano, A. Sclafani, Physico-chemical properties of WO<sub>3</sub>/TiO<sub>2</sub> systems employed for 4-nitrophenol photodegradation in aqueous medium, Catal. Lett. 49 (1997) 235–243.
- [15] N. Serpone, P. Maruthamuthu, P. Pichat, E. Pelizetti, H. Hidaka, Exploiting the interparticle electron transfer process in the photocatalysed oxidation of phenol, 2-chlorophenol and pentachlorophenol: chemical evidence for electron and hole transfer between coupled semiconductors, J. Photochem. Photobiol. A: Chem. 85 (1995) 247–255.
- [16] V. Keller, F. Garin, Photocatalytic behavior of a new composite ternary system: WO<sub>3</sub>/SiC-TiO<sub>2</sub>. Effect of the coupling of semiconductors and oxides in photocatalytic oxidation of methylethylketone in the gas phase, Catal. Commun. 4 (2003) 377–383.
- [17] Å.D. Paola, L. Palmisano, V. Augugliari, Photocatalytic behavior of mixed  $WO_3/WS_2$  powders, Catal. Today 58 (2000) 141–149.
- [18] H. Irie, Y. Watanabe, K. Hashimoto, Carbon-doped anatase TiO<sub>2</sub> powders as a visible-light sensitive photocatalyst, Chem. Lett. 32 (2003) 772–773.
- [19] R. Asahi, T. Morikawa, T. Ohwaki, K. Aoki, Y. Taga, Visible-light photocatalysis in nitrogen-doped titanium oxides, Science 293 (2001) 269–271.
- [20] T. Ohno, M. Akiyoshi, T. Umebayashi, K. Asai, T. Mitsui, M. Matsumura, Preparation of S-doped TiO<sub>2</sub> photocatalysts and their photocatalytic activities under visible light, Appl. Catal. A 265 (2004) 115–121.
- [21] J.C. Yu, J.G. Yu, W.K. Ho, Z. Jiang, L.Z. Zhang, Effects of F-dopingon the photocatalytic activity and microstructures of nanocrystalline TiO<sub>2</sub> powders, Chem. Mater. 14 (2002) 3808–3816.
- [22] D.M. Chen, D. Yang, Q. Wang, Z.Y. Jiang, Effects of boron doping on photocatalytic activity and microstructure of titanium dioxide nanoparticles, Ind. Eng. Chem. Res. 45 (2006) 4110–4116.
- [23] W.K. Jo, J.T. Kim, Application of visible-light photocatalysis with nitrogendoped or unmodified titanium dioxide for control of indoor-level volatile organic compounds, J. Hazard. Mater. 164 (2009) 360–366.
- [24] D. Kibanova, J. Cervini-Silva, H. Destaillats, Efficiency of clay-TiO<sub>2</sub> nanocomposites on the photocatalytic elimination of a model hydrophobic air pollutant, Environ. Sci. Technol. 43 (2009) 1500–1506.

- [25] M. Sleiman, P. Conchon, C. Ferronato, J.M. Chovelon, Photocatalytic oxidation of toluene at indoor air levels (ppbv): towards a better assessment of conversion, reaction intermediates and mineralization, Appl. Catal. B Environ. 86 (2009) 159-165
- [26] Fan Dong, Weirong Zhao, Zhongbiao Wu, Sen Guo, Band structure and visible light photocatalytic activity of multi-type nitrogen doped TiO<sub>2</sub> nanoparticles prepared by thermal decomposition, J. Hazard. Mater. 162 (2009) 763–770.
- [27] S.J. Hwang, H.M. Tang, Kinetic behavior of the toluene biofiltration process, J. Air Waste Manage, Assoc, 47 (1997) 664–673.
- [28] M.C. Delhomienie, L. Bibeau, N. Bredin, S. Roy, S. Broussau, R. Brzezinski, J.L. Kugelmass, M. Heitz, Biofiltration of air contaminated with toluene on a compost-based bed, Adv. Environ. Res. 6 (2002) 239–254.
- [29] R.S. Singh, S.S. Agnihotri, S.N. Upadhyay, Removal of toluene vapour using agrowaste as biofilter media, Bioresour. Technol. 97 (2006) 2296–2301.
- [30] H.T. Znad, K. Katoh, Y. Kawase, High loading toluene treatment in a compost based biofilter using up-flow and down-flow swing operation, J. Hazard. Mater. 141 (2007) 745–752.
- [31] A. Kumar, J. Dewulf, A. Vercruyssen, H.V. Langenhove, Performance of a composite membrane bioreactor treating toluene vapors: inocula selection, reactor performance and behavior under transient conditions, Bioresour. Technol. 100 (2009) 2381–2387.
- [32] A. Kumar, J. Dewulf, M. Luvsanjamba, H.V. Langenhove, Continuous operation of membrane bioreactor treating toluene vapors by *Burkholderia vietnamiensis* G4, Chem. Eng. J. 140 (2008) 193–200.
- [33] F. Arsac, D. Bianchi, J.M. Chovelon, P. Conchon, C. Ferronato, A. Lair, M. Sleiman, Photocatalytic degradation of organic pollutants in water and in air. An analytical approach, Mater. Sci. Eng. C 28 (2008) 722–725.
- [34] J.H. Mo, Y.P. Zhang, Q.J. Xu, Y.F. Zhu, J.J. Lamson, R.Y. Zhao, Determination and risk assessment of by-products resulting from photocatalytic oxidation of toluene, Appl. Catal. B Environ. 89 (2009) 570–576.
- [35] S. Ardizzone, C.L. Bianchi, G. Cappelletti, A. Naldoni, C. Pirola, Photocatalytic degradation of toluene in the gas phase: relationship between surface species and catalyst features, Environ. Sci. Technol. 42 (2008) 6671–6676.

- [36] C. Di Valentin, G. Pacchioni, A. Selloni, S. Livraghi, E. Giamello, Characterization of paramagnetic species in N-doped TiO<sub>2</sub> powders by EPR spectroscopy and DFT calculations, J. Phys. Chem. B 109 (2005) 11414–11419.
- [37] J.G. Yu, H.G. Yu, B. Cheng, X.J. Zhao, J.C. Yu, W.K. Ho, The effect of calcinations temperature on the surface microstructure and photocatalytic activity of TiO<sub>2</sub> thin films prepared by liquid phase deposition, J. Phys. Chem. B 107 (2003) 13871–13879.
- [38] J.G. Yu, G.H. Wang, B. Cheng, M.H. Zhou, Effects of hydrothermal temperature and time on the photocatalytic activity and microstructures of bimodal mesoporous TiO<sub>2</sub> powders, Appl. Catal. B 69 (2007) 171–180.
- [39] S. Livraghi, M.C. Paganini, E. Giamello, A. Selloni, C. Di Valentin, G. Pacchioni, Origin of photoactivity of nitrogen-doped titanium dioxide under visible light, J. Am. Chem. Soc. 128 (2007) 15666–15671.
- [40] F. Wei, L. Ni, P. Cui, Preparation and characterization of N-S-codoped TiO<sub>2</sub> photocatalyst and its photocatalytic activity, J. Hazard. Mater. 156 (2008) 135–140
- [41] H. Li, J. Li, Y. Huo, Highly active TiO<sub>2</sub> N photocatalysts prepared by treating TiO<sub>2</sub> precursors in NH<sub>3</sub>/ethanol fluid under supercritical conditions, J. Phys. Chem. 110B (2006) 1559–1565.
- [42] M.C. Blount, J.L. Falconer, Steady-state surface species during toluene photocatalysis, Appl. Catal. B Environ. 39 (2002) 39–50.
- [43] H. Einaga, S. Futamura, T. Ibusuki, Heterogeneous photocatalytic oxidation of benzene, toluene, cyclohexene and cyclohexane in humidified air: comparison of decomposition behavior on photoirradiated TiO<sub>2</sub> catalyst, Appl. Catal. B Environ. 38 (2002) 215–225.
- [44] V. Augugliaro, S. Coluccia, V. Lodoo, G. Martha, L. Palmisano, M. Schiavello, Photocatalytic oxidation of gaseous toluene on anatase TiO<sub>2</sub> catalyst: mechanistic aspects and FT-IR investigation, Appl. Catal. B Environ. 20 (1999) 15–27.
- [45] Y. Irokawa, T. Morikawa, K. Aoki, S. Kosaka, T. Ohwaki, Y. Taga, Photodegradation of toluene over TiO<sub>2-x</sub>N<sub>x</sub> under visible light irradiation, Phys. Chem. Chem. Phys. 8 (2006) 1116–1121.
- [46] S.B. Kim, S.C. Hong, Kinetic study for photocatalytic degradation of volatile organic compounds in air using thin film TiO<sub>2</sub> photocatalyst, Appl. Catal. B Environ. 35 (2002) 305–315.